IOPscience iopscience.iop.org

Home Search Collections Journals About Contact us My IOPscience

Hole doping effects in $Sr_2FeMo_{1-x}W_xO_6$ ($0 \leq x \leq 1$) double perovskites: a neutron diffraction study

This article has been downloaded from IOPscience. Please scroll down to see the full text article.

2005 J. Phys.: Condens. Matter 17 3673

(http://iopscience.iop.org/0953-8984/17/23/019)

View the table of contents for this issue, or go to the journal homepage for more

Download details:
IP Address: 129.252.86.83
The article was downloaded on 28/05/2010 at 04:59

Please note that terms and conditions apply.

INSTITUTE OF PHYSICS PUBLISHING JOURNAL OF PHYSICS: CONDENSED MATTER

J. Phys.: Condens. Matter **17** (2005) 3673–3688 doi:10.1088/0953-8984/17/23/019

Hole doping effects in $Sr_2FeMo_{1-x}W_xO_6$ ($0 \leqslant x \leqslant 1$) double perovskites: a neutron diffraction study

D Sánchez, J A Alonso[1], M García-Hernández, M J Martínez-Lope and M T Casais

Instituto de Ciencia de Materiales de Madrid, CSIC, Cantoblanco, E-28049 Madrid, Spain

E-mail: ja.alonso@icmm.csic.es

Received 25 January 2005, in final form 6 May 2005
Published 27 May 2005
Online at stacks.iop.org/JPhysCM/17/3673

Abstract

The effect of the localization of electrons as Mo is substituted by W in the $Sr_2FeMo_{1-x}W_xO_6$ ($0 \leqslant x \leqslant 1$) series has been studied by neutron powder diffraction (NPD) and SQUID magnetometry. The samples for $x = 0.2, 0.5, 0.8$ and 1 were prepared by soft-chemistry procedures and annealed under suitable reducing conditions for each member of the series. As the number of itinerant electrons drastically changes from Sr_2FeMoO_6 (one electron per formula unit) to Sr_2FeWO_6 (no itinerant electrons), this series constitutes an ideal system to explore band filling effects in the magnetic structure and the Curie temperature of half-metallic ferromagnetic double perovskites. The room-temperature crystal structure of the former members of the series ($x \leqslant 0.5$) is tetragonal ($I4/m$) and it is characterized by a single antiphase tilt of the FeO_6 and (Mo, W)O_6 octahedra along the c axis; this structure evolves to the more distorted monoclinic ($P2_1/n$) for $x = 0.8$ and 1, containing three kinds of non-equivalent oxygen atoms. The driving force of the structural phase transition is the promotion of the voluminous Fe^{2+} cations upon W substitution, as demonstrated by a bond valence study. The phase transition is accompanied by a sudden decrease of the distortion of the FeO_6 and (Mo, W)O_6 octahedra. Our results show that the progressive localization of carriers upon W substitution provides a good description of the magnetic and structural properties along the series. The study of the low-temperature (10 K) NPD pattern of the heavily W-doped $Sr_2FeMo_{0.2}W_{0.8}O_6$ suggests a lack of long-range magnetic ordering, which is consistent with the presence of isolated ferromagnetic clusters in the insulating, antiferromagnetic matrix created by Fe–O–W–O–Fe superexchange interactions.

(Some figures in this article are in colour only in the electronic version)

[1] Author to whom any correspondence should be addressed.

0953-8984/05/233673+16$30.00 © 2005 IOP Publishing Ltd Printed in the UK

1. Introduction

Among the family of double-perovskite oxides $A_2B'B''O_6$, only a few compounds exhibit the attractive half-metallic ferromagnetic state characterized by a high transition temperature, such as Sr_2FeMoO_6. Indeed, such a state is somewhat unexpected in this oxide, since the magnetic ions are placed far apart in the structure, suggesting a weak direct magnetic interaction. Moreover, such interactions between d ions mediated via other non-magnetic ions are expected to be antiferromagnetic due to a superexchange mechanism. This expectation is supported by the observation of an antiferromagnetic, insulating ground state of the closely related system Sr_2FeWO_6, with a Néel temperature of 37 K. However, in the case of Sr_2FeMoO_6 and other ferromagnetic double perovskites, a mechanism based on the indirect coupling of the magnetic ions through itinerant electrons is thought to account for the encountered high-T_C ferromagnetism [1–3]. Photoemission spectroscopy experiments [1, 4–6], x-ray absorption spectroscopy [7] and magnetic measurements in the paramagnetic phase [3] have supported this idea.

From the theoretical point of view, the scheme of interactions proposed by Sarma *et al* [1] seems to be broadly accepted. Within this scenario, ferromagnetism and half metallicity are determined by the competition between electron hopping processes and localization of electrons at the bare levels of the transition metal cations. Also, the ferromagnetic ordering can be understood as resulting from the interaction of the localized spins at the Fe sites with the spin-polarized electrons in the conduction band. Thus, ferromagnetism in this material does not arise from the direct interaction of the localized magnetic moments between each other, but from the indirect interaction through the itinerant carriers.

In the framework of the proposed model [1], the stabilization of such a spin-polarized conduction band, and thus of a ferromagnetically ordered state, mostly depends on the B′/B″ (Fe/Mo) site energy difference [1, 8, 9] and the hopping interaction strengths between B′ and B″ cations [10, 11]. In turn, the site energy difference is controlled by the exchange interactions, crystal field splitting and degree of hybridization with the oxygen orbitals [1, 4] of the cations occupying B′ and B″ positions. Obviously, the hopping interaction strengths depend on the structural parameters, like B′–O, B″–O distances and B′–O–B″ bond angles. Also, the number of carriers in the conduction band seems to play a role in stabilizing the ferromagnetic state.

Several theoretical approaches based on different calculation methods can be found in the literature [1, 8, 9, 12], all of them pointing out the fundamental relevance of itinerant carriers in the stabilization of the long-range ferromagnetic ordering in double perovskites. In addition to this, it is proposed that the contribution of a small number of antisite defects ($y \sim 0.05$) is necessary to reinforce ferromagnetism [12, 13].

Within Sarma's scheme, there can also be configurations in which the matching of the B′ and B″ site energies does not favour the stabilization of the conduction band, as in Sr_2FeWO_6. Due to a larger hybridization with the oxygen orbitals, the W $t_{2g\downarrow}$ states appear above Fe $e_{g\downarrow}$ states, ruling out the possibility to stabilize the Fe $t_{2g\downarrow}$–O(2p)–W $t_{2g\downarrow}$ conduction band [14]. In contrast, the W 5d electron is totally transferred to Fe orbitals.

Among the various parameters controlling the appearance of a ferromagnetic state in ordered double perovskites, band filling effects have attracted much attention [15–19]. The hypothesized stabilization of the ferromagnetic ordering via electron hopping brings about the possibility of tuning T_C by changing the band filling in Sr_2FeMoO_6. This can be achieved by chemical substitutions in the parent compound. As the ordering temperature determines the highest operation temperature of devices based on these materials, this possibility is fairly interesting from the practical point of view.

However, the sole effect of the population of the conduction band in T_C is still quite controversial, given the spread in the experimentally reported values of T_C in the electron doped $Sr_{2-x}La_xFeMoO_6$ series [15, 19, 20], the disagreement with the predictions of theoretical models [9] and, especially, the concomitant appearance of anti-site defects as electron doping increases [15, 16, 19].

In the $Sr_2FeMo_{1-x}W_xO_6$ ($0 \leqslant x \leqslant 1$) series, the localization of electrons as Mo is substituted by W gives rise to an effective decrease in the number of itinerant carriers, in spite of the fact that Sr_2FeMoO_6 and Sr_2FeWO_6 are isoelectronic. Also, antisite disorder effects are thought to be minimized in this series, because the introduction of the highly charged W^{6+} cation favours the B′/B″ ordering.

The two limiting cases for the solid solution $Sr_2FeMo_{1-x}W_xO_6$ ($0 \leqslant x \leqslant 1$) have very different magnetic and transport properties. Sr_2FeWO_6 is insulating in the whole temperature range, and it exhibits antiferromagnetic ordering below $T_N \sim 37$ K [21–23]. This compound, in contrast to Sr_2FeMoO_6, contains W^{6+} ($5d^0$) and Fe^{2+} ($3d^6$) species [21, 22, 24]. Here, in the absence of d itinerant electrons, the Fe^{2+} ions are believed to couple to each other via Fe–O–W–O–Fe super-superexchange interactions, which are antiferromagnetic. One of the possible scenarios to explain the observed results in $Sr_2FeMo_{1-x}W_xO_6$ ($0 \leqslant x \leqslant 1$) series is the collective valence transition from $Fe^{3+}W^{5+}$ to $Fe^{2+}W^{6+}$ at a critical concentration x_c [25]. Rather to the contrary, other works suggest that Mo and W always remain as Mo^{5+} and W^{6+} respectively [23], implying that there is no valence transition but a continuous decrease in the number of itinerant electrons per formula unit. This has also been pointed out in [24], where an almost linear decrease of the mixed valence component $Fe^{2.5+}$ in the Mössbauer spectra is observed when increasing the W content in $Sr_2FeMo_{1-x}W_xO_6$. This series has been previously studied from the magnetic and transport points of view, with special attention to the metal–insulator transition at a certain x, and the magnetoresistive effects arising in the proximity of such a critical concentration [23, 25]. Reference [23] reports on a x-ray diffraction study of the unit-cell parameters for a large number of x values in this series; however, the structural changes have not been investigated in detail by neutron diffraction, which can be enlightening concerning the evolution of the electronic structure in the compounds. This is the main goal of this study.

We have studied the series $Sr_2FeMo_{1-x}W_xO_6$ with ($0 \leqslant x \leqslant 1$) by SQUID magnetometry and neutron diffraction. One of our aims is to elucidate whether the valence transition model or the progressive localization of carriers upon W substitution provides a better description of the magnetic and structural properties along the series. As the number of itinerant electrons drastically changes from Sr_2FeMoO_6 (1 electron per formula unit) to Sr_2FeWO_6 (no itinerant electrons), this series constitutes an ideal system to explore band filling effects in the magnetic structure and the Curie temperature of half-metallic ferromagnetic double perovskites. Furthermore, many authors have reported an enhanced ordering level upon W-substitution in Sr_2FeMoO_6, due to the increase in the B′/B″ charge difference for the $Fe^{2+}W^{6+}$ configuration compared to the nominal $Fe^{3+}Mo^{5+}$ one [23, 25–27]. Thus, in contrast to the electron-doped series, anti-site disorder effects are thought to be minimized along the $Sr_2FeMo_{1-x}W_xO_6$ series.

2. Experimental details

The series $Sr_2FeMo_{1-x}W_xO_6$ ($x = 0.2, 0.5, 0.8, 1$) was prepared by soft-chemistry procedures. Stoichiometric amounts of analytical grade $Sr(NO_3)_2$, $FeC_2O_4{\cdot}2H_2O$, $(NH_4)_6Mo_7O_{24}{\cdot}4H_2O$ and $H_{26}N_6O_{41}W_{12}{\cdot}18H_2O$ were dissolved in citric acid. The citrate + nitrate solutions were slowly evaporated, leading to organic resins containing a

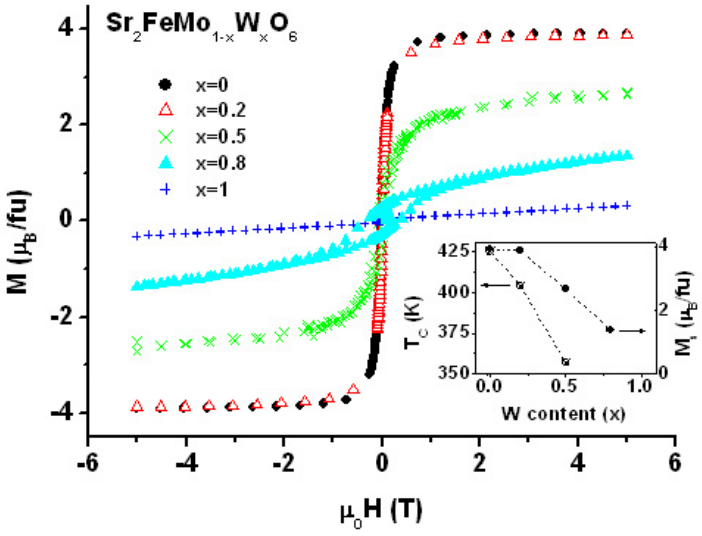

Figure 1. Hysteresis loops of the $Sr_2FeMo_{1-x}W_xO_6$ ($0 \leqslant x \leqslant 1$) series at 5 K. Inset, evolution of the Curie temperature (left) and magnetization at 5 T and 5 K (right) in the $Sr_2FeMo_{1-x}W_xO_6$ ($0 \leqslant x \leqslant 1$) series.

homogeneous distribution of the involved cations. These resins were first dried at 120 °C and then slowly decomposed at temperatures up to 600 °C for 12 h. For the $x = 0.2, 0.5$ compounds, the precursors were annealed at 820 °C for 6 h in a H_2/N_2 (5%/95%) reducing flow. The $x = 0.8$ sample was treated at 900 °C in a H_2/Ar (1%/99%) flow for 6 h. The end of the series, Sr_2FeWO_6, was heated in H_2/N_2 (5%/95%) at 1000 °C for 6 h. The $x = 0$ compound, Sr_2FeMoO_6, has been prepared as described in [28]. The degree of ordering obtained from XRD was found to be greater than 90% in all the samples.

The DC magnetic characterization of the samples was done in a SQUID magnetometer (Quantum Design), in the temperature range 5–400 K. The magnetization was measured in field cooled (FC) samples at 1000 Oe. Neutron powder diffraction diagrams were collected at the ILL in Grenoble. The nuclear structures were refined from the high resolution NPD patterns, acquired at room temperature at the D2B diffractometer ($\lambda = 1.594$ Å). To study the magnetic structure of the highly substituted sample $Sr_2FeMo_{0.2}W_{0.8}O_6$, additional data at 10 K were also taken at D2B. For the study of the thermal evolution of the magnetic and nuclear structure of the Sr_2FeWO_6 ($x = 1$) compound, a series of NPD patterns was obtained at the D20 high-flux diffractometer (also at the ILL) with a wavelength of 2.42 Å, in the temperature range from 20 to 70 K. The refinements of both crystal and magnetic structures were performed by the Rietveld method, using the FullProf refinement program [29].

3. Results and discussion

3.1. Magnetic properties

The hysteresis loops for the $Sr_2FeMo_{1-x}W_xO_6$ ($0 \leqslant x \leqslant 1$) series are shown in figure 1. The $x = 0$ and 0.2 samples show almost full magnetization, 3.90 and 3.87 μ_B fu^{-1} respectively. For $x > 0.2$, M_s is considerably reduced when increasing x. For the highly substituted samples ($x = 0.8$ and 1) the magnetization is still not saturated at a field of 5 T, indicating the

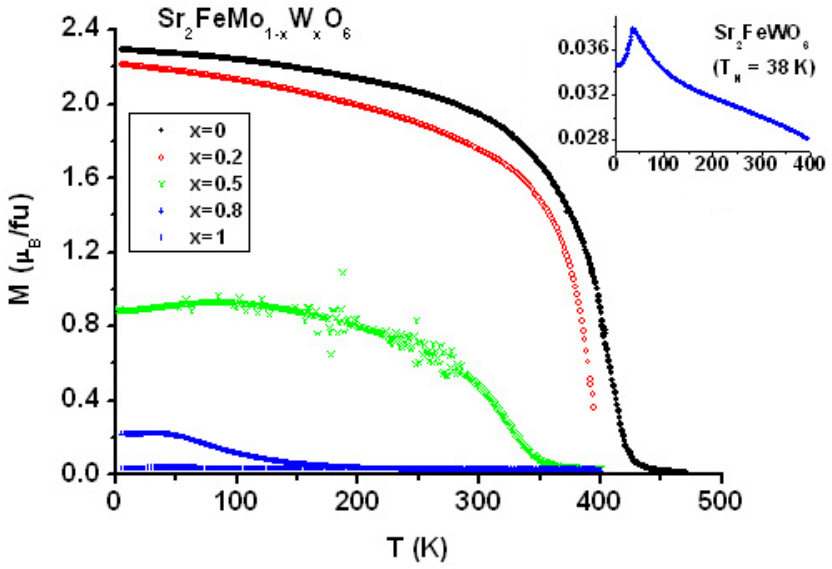

Figure 2. Magnetization versus temperature curves of the $Sr_2FeMo_{1-x}W_xO_6$ ($0 \leqslant x \leqslant 1$) series at 1000 Oe. The inset shows the antiferromagnetic behaviour of the Sr_2FeWO_6 sample ($x = 1$), with $T_N = 38$ K.

disappearance of the long-range ferromagnetic ordering. Previous reports [23, 25] describe a systematic increase of M_s with x, reaching the highest moment for $Sr_2FeMo_{0.4}W_{0.6}O_6$ [23] or $Sr_2FeMo_{0.3}Mo_{0.3}W_{0.7}O_6$ [25]; this is due to serious anti-site Fe/Mo disordering effects encountered for the reported $x = 0$ material, in such a way that the introduction of W^{6+} cations improves the B-site ordering and thus M_s regularly increases in the lower W-doping region [23, 25]. This is in contrast with our more perfectly B-site ordered materials, reaching exceptionally high saturation magnetizations up to 3.90 and 3.87 μ_B fu^{-1} for the $x = 0$ and 0.2 samples, respectively.

The evolution of the magnetic behaviour in the $Sr_2FeMo_{1-x}W_xO_6$ ($0 \leqslant x \leqslant 1$) series is also displayed in figure 2, showing the susceptibility curves of the samples at 1000 Oe. The ferromagnetic ordering temperature in the samples with $x \leqslant 0.5$ clearly decreases when increasing W substitution. For $x = 0.5$, the magnetization already shows a slight decrease below 100 K, probably arising from the progressive appearance of AFM interactions. Further increase in the W content leads to a long-range AFM ordering, which is first evidenced by a small cusp at ~34 K in the $M(T)$ curve from the $x = 0.8$ sample. A clear Néel peak is observed in the extreme of the series ($x = 1$) (inset of figure 2) at $T_N = 38$ K.

The results concerning the evolution of the Curie temperature and the saturation magnetization with x are summarized as an inset in figure 1. Notice that only the T_C for samples up to $x = 0.5$, exhibiting a clear FM behaviour, are represented. In agreement with reported results [23, 24], T_C decreases with the W content. A reduction in the saturation magnetization is also observed, as a consequence of the appearance of Fe–O–W–O–Fe pairs.

3.2. NPD structural characterization

The reported structural studies in $Sr_2FeMo_{1-x}W_xO_6$ ($0 \leqslant x \leqslant 1$) are based on x-ray diffraction analysis [23, 24, 26, 27]. Only the limiting compounds of the series, Sr_2FeMoO_6 and

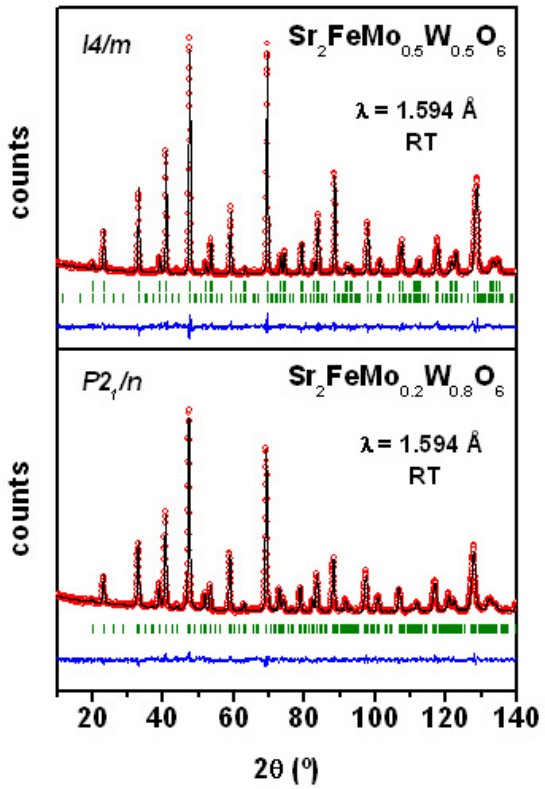

Figure 3. Room-temperature NPD patterns and Rietveld refinements for $Sr_2FeMo_{0.5}W_{0.5}O_6$ (upper) and $Sr_2FeMo_{0.2}W_{0.8}O_6$ (lower) samples. The second series of tick marks corresponds to the magnetic structure.

Sr_2FeWO_6, have been accurately studied by neutron diffraction [30, 31]. Sr_2FeWO_6 was first characterized as cubic [32], and a later study suggested a tetragonal structure [21] after XRD measurements at room temperature. In the more recent results in [23, 24], the compound is characterized as cubic and 'almost cubic' respectively, while a tetragonal symmetry is found in all the $Sr_2FeMo_{1-x}W_xO_6$ ($0 \leqslant x \leqslant 1$) series in [26]. A neutron diffraction study, more sensitive to the positions of the oxygen atoms, shows that the Sr_2FeWO_6 compound adopts a monoclinic symmetry (space group $P2_1/n$) from 10 K to room temperature [31]. It has been shown that the $x = 0$ compound, Sr_2FeMoO_6, is perfectly described in the tetragonal $I4/m$ space group [19, 30]. The tetragonal distortion arises from the anti-phase rotation of the oxygen octahedra with respect to the c-axis ($a^0a^0c^-$ in Glazer's notation [33]). Then, in the $Sr_2FeMo_{1-x}W_xO_6$ ($0 \leqslant x \leqslant 1$) series, a structural transition from tetragonal to monoclinic symmetry is expected at a certain x.

The crystal structure refinement was performed on the D2B high-resolution data at room temperature. We have refined the structure of samples up to $x = 0.5$ in the tetragonal $I4/m$ group. The NPD data for the $x = 0.8$ and 1 samples could not be satisfactorily fitted within a tetragonal symmetry, and the structures have been refined in the monoclinic $P2_1/n$ space group. For the samples exhibiting a clear ferromagnetic behaviour after SQUID measurements ($x = 0$, 0.2 and 0.5), the refinements were improved when a magnetic phase was included in the model. The goodness of the refinements along the series is shown in figure 3. The most

Table 1. Main structural parameters and agreement factors from the Rietveld refinement of the room-temperature structures of $Sr_2FeMo_{1-x}W_xO_6$ ($0 \leqslant x \leqslant 1$) from NPD data.

Sample	$x = 0$	$x = 0.2$	$x = 0.5$		$x = 0.8$	$x = 1$
$I4/m$				$P2_1/n$		
a (Å)	5.56846(5)	5.5753(1)	5.58700(9)	a (Å)	5.6347(3)	5.6508(1)
b (Å)	5.56846(5)	5.5753(1)	5.58700(9)	b (Å)	5.6082(3)	5.6136(1)
c (Å)	7.9004(1)	7.9122(3)	7.9328(2)	c (Å)	7.9252(4)	7.9425(2)
				β (deg)	90.05(1)	90.021(5)
V (Å^3)	244.976(4)	245.94(1)	247.618(9)	V (Å^3)	250.44(2)	251.944(9)
Sr 4d(1/2 0 1/4)				Sr 4e(x y z)		
B (Å^2)	0.93(2)	0.77(6)	0.86(2)	x	1.000(1)	0.9990(7)
				y	0.009(1)	0.0129(8)
				z	0.247(2)	0.2491(9)
				B (Å^2)	1.10(3)	0.87(3)
Fe 2a(0 0 0)				Fe 2d(1/2 0 1/2)		
B (Å^2)	0.81(9)	0.5(3)	1.5(1)	B (Å^2)	1.0(1)	0.36(8)
Mag. mom. (μ_B)	1.7(8)	2.6(3)	1.0(1)	Mag. mom. (μ_B)	—	—
Mo 2b(0 0 1/2)				Mo 2b(1/2 0 0)		
B (Å^2)	0.0(1)	0.4(4)	−0.8(8)	B (Å^2)	0.2(2)	0.6(2)
Mag. mom. (μ_B)	−0.8(3)	−0.2(2)	—	Mag. mom. (μ_B)	—	—
O1 4e(0 0 z)				O1 4e(x y z)		
z	0.254(1)	0.255(3)	0.2622(6)	x	0.0441(8)	0.0473(5)
B (Å^2)	1.00(5)	0.9(1)	0.72(7)	y	0.511(1)	0.496(1)
				z	0.257(2)	0.259(1)
				B (Å^2)	0.8(1)	0.97(9)
O2 8h(x y 0)				O2 4e(x y z)		
x	0.2719(8)	0.272(2)	0.2751(8)	x	0.719(1)	0.719(1)
y	0.2332(6)	0.233(2)	0.2281(8)	y	0.261(2)	0.261(1)
B (Å^2)	1.05(2)	0.89(8)	1.14(4)	z	0.0286(8)	0.025(1)
				B (Å^2)	1.2(2)	1.0(2)
				O3 4e(x y z)		
				x	0.248(1)	0.242(1)
				y	0.235(2)	0.224(1)
				z	0.984(1)	0.976(1)
				B (Å^2)	1.2(1)	1.1(2)
Reliability factors						
χ^2	2.96	11.9	1.84	χ^2	1.74	1.56
R_p (%)	3.98	7.25	4.10	R_p (%)	3.16	3.51
R_{wp} (%)	5.05	17.3	5.17	R_{wp} (%)	3.98	4.67
R_I (%)	3.04	6.32	3.51	R_I (%)	4.52	5.38
$R_{mag.}$ (%)	10.5	20.0	16.9	$R_{mag.}$ (%)	—	—

relevant structural parameters, the ordered magnetic moments and the agreement factors are given in table 1.

As happens in the La-doped series, and in many other 1:1 ordered double perovskites [34–36], a monoclinic angle β close to 90° reveals a strong pseudo-orthorhombic character. The evolution of the lattice parameters a, b and c and the cell volume with the W content x is shown in figure 4. A continuous cell expansion upon W substitution is observed, in

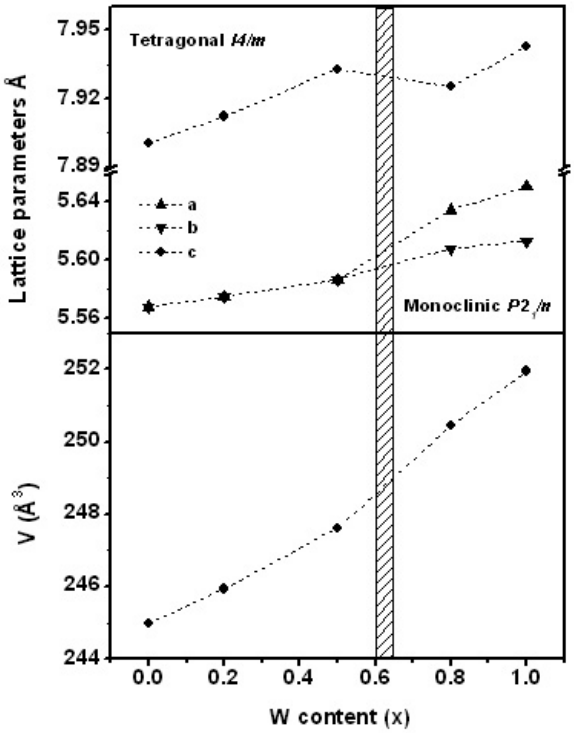

Figure 4. Evolution of the lattice parameters and volume in the $Sr_2FeMo_{1-x}W_xO_6$ ($0 \leqslant x \leqslant 1$) series at room temperature.

agreement with previous observations [23, 24, 26]. If we assume that $Fe^{2+}W^{6+}$ configurations replace the nominal $Fe^{3+}Mo^{5+}$ state, such a cell expansion should be expected since the ionic radius of Fe^{2+} (0.78 Å in VI-fold coordination) is remarkably larger than that of the high-spin Fe^{3+} cation (0.645 Å) [37]. In other words, as pointed out in [26], the progressive localization of the carriers induces an increase in the cell volume. However, these authors attribute the cell expansion to the localization of carriers only for samples with $x > 0.3$, as indicated by a minimum in the reported c axis versus x curve. Our results suggest that the cell expansion holds in the whole x range, given the smooth evolution of the volume and the lattice parameters with the W content.

It is worth noting that the minimum in c at $x = 0.8$ observed in figure 4 does not have a physical meaning, but is just a consequence of the cell choice in the monoclinic $P2_1/n$ group (unique axis c, cell choice 2): the monoclinic c axis within this setting is not equivalent to the tetragonal c axis in the $I4/m$ group, since the rotation of the BO_6 octahedra is in antiphase for the tetragonal phase, and in phase for the monoclinic phase.

Then, the lattice constants in the monoclinic $P2_1/n$ setting have been recalculated to describe the structural transition in a continuous way. The appropriate choice of the pseudocubic axes is depicted in figure 5. This choice accounts for the in-phase octahedra tilting along the (100) direction of the pseudocubic cell, and in antiphase along the (010) and (001) directions, which corresponds to the $a^+b^-b^-$ Glazer notation as derived by Woodward [34] for 1:1 ordering in double perovskites, consistent with space group $P2_1/n$. After the appropriate calculation of the pseudocubic a, b and c parameters in the tetragonal and the monoclinic

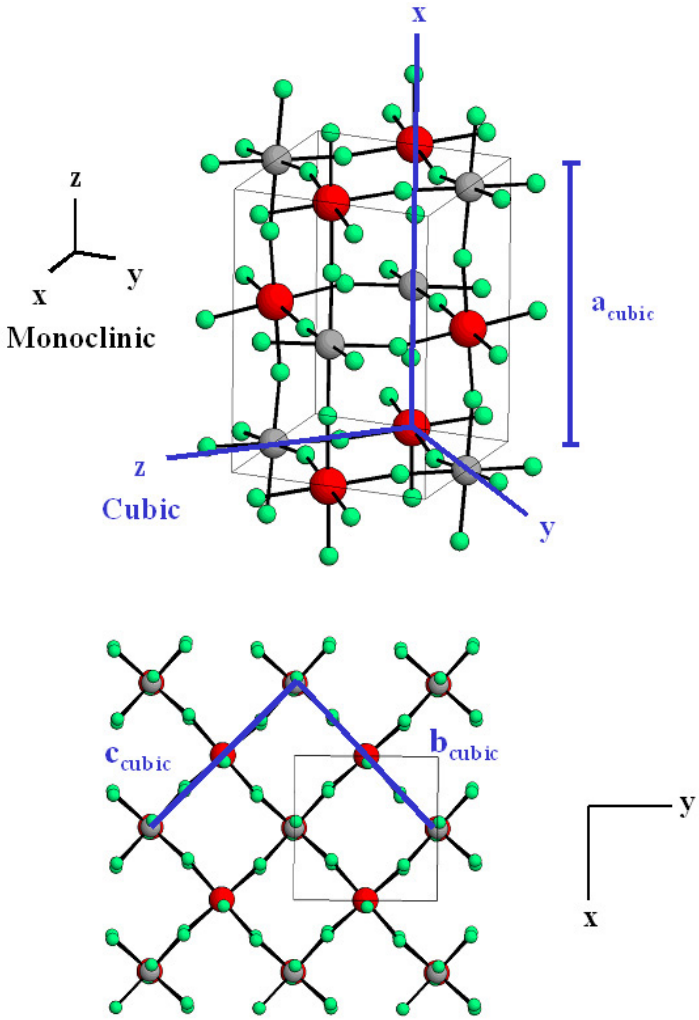

Figure 5. Pseudocubic axis in the monoclinic setting $P2_1/n$ (unique axis c, cell choice 2).

phase, the evolution of the lattice constants with x is continuous and smooth, as shown in figure 6.

The parameters given in figure 7 reveal that the driving force of the structural phase transition is the promotion of the voluminous Fe^{2+} cations upon W substitution, as will be discussed in the following. It should be noticed that the ionic radii of Mo^{5+} (0.61 Å) and W^{6+} (0.60 Å) are very similar [37].

If the tolerance factor is approximately estimated as

$$t = \frac{r_A + r_O}{\sqrt{2}\left(\frac{r_{B'} + r_{B''}}{2} + r_O\right)},$$

with

$$r_{B'} = (1 - x)r_{Fe^{3+}} + xr_{Fe^{2+}}$$

$$r_{B''} = (1 - x)r_{Mo^{5+}} + xr_{W^{6+}},$$

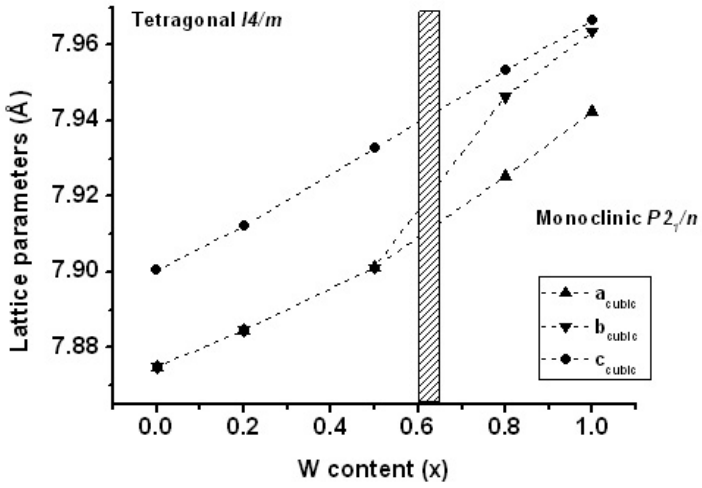

Figure 6. Evolution of the pseudocubic lattice parameters a, b and c with x.

it changes from $t = 0.998$ in Sr_2FeMoO_6 to $t = 0.973$ in the $Sr_2FeMo_{0.2}W_{0.8}O_6$ sample, accounting for the change of symmetry. A microscopic approach based on the calculated bond distances can be extracted from figure 7: after an Fe atom has received the $5d^1$ electron transferred from a substituting W atom, the FeO_6 octahedra expands along the out-of-plane direction while the (Mo, W)O_6 octahedra contracts (figure 7(a)). The Coulomb energy gain is compensated in the basal plane by increasing the antiphase rotation of the octahedra along the c axis (figure 7(d)), keeping the in-plane bond distances almost unchanged (figure 7(a)). This provokes a strong distortion of the BO_6 octahedra (figure 7(b)), and a strong increase in the metal–oxygen bond tensile stress with increasing x. The distortion Δ in figure 7(b) is calculated as

$$\Delta = \frac{1}{N}\sum_{n=1,N}\left[\frac{d_n - \langle d\rangle}{\langle d\rangle}\right]^2$$

where n runs over the number of ligands N (oxygen atoms, $N = 6$ for Fe and Mo and $N = 12$ for Sr); d_n denotes a particular metal–oxygen distance and $\langle d\rangle$ is the average metal–oxygen distance.

At a high substitution level, $x \sim 0.6$, the BO_6 octahedra tilt to relax the bond stress, and the compound undergoes a change of symmetry. As seen in figures 7(a) and (b), the BO_6 distortion is minimized after the structural phase transition. This translates into a distortion of the Sr environment (figure 7(c)), accommodating the changes in the metal–oxygen octahedra within the 12 Sr–O bonds. The calculated bond distances and bond angles are summarized in table 2.

The oxidation states in Fe and (Mo, W) sites have been calculated through Brown's bond valence model [38, 39]. The results in figure 8 support the progressive conversion of the nominal configuration $Fe^{3+}Mo^{5+}$ into $Fe^{2+}W^{6+}$ with increasing x, ruling out the existence of a valence transition at a certain x.

3.3. Magnetic structures in highly substituted samples

3.3.1. $Sr_2FeMo_{0.2}W_{0.8}O_6$. A first exploration of the high-resolution NDP pattern of $Sr_2FeMo_{0.2}W_{0.8}O_6$ at 10 K suggests the lack of long-range magnetic ordering, since all the

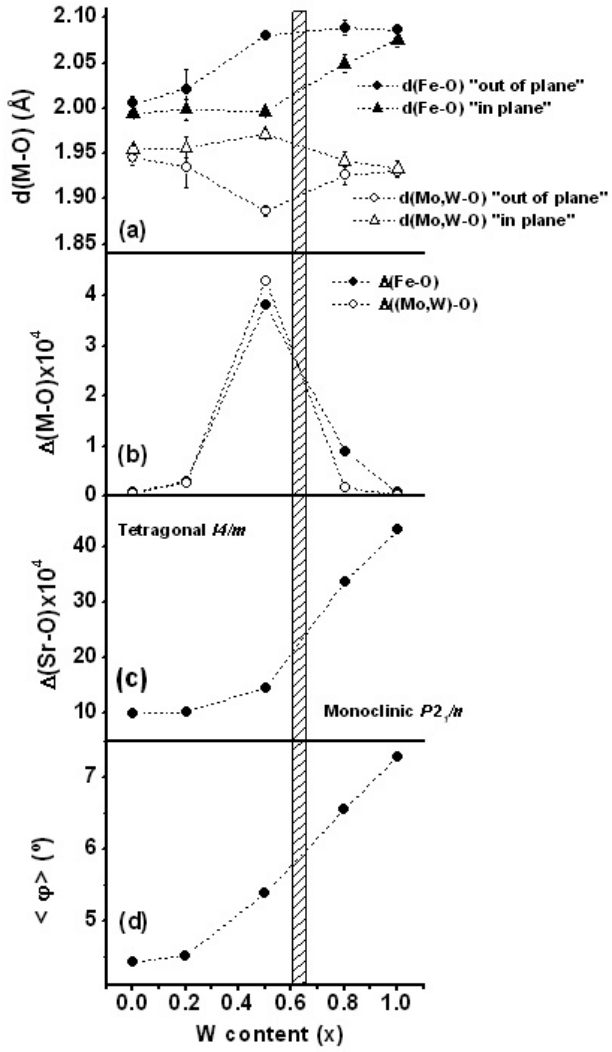

Figure 7. (a) Calculated metal–oxygen bond distances; (b) BO_6 octahedron distortion, calculated as defined in the text; (c) distortion of the Sr–O environment; (d) average tilting of the BO_6 octahedra along the $Sr_2FeMo_{1-x}W_xO_6$ ($0 \leqslant x \leqslant 1$) series.

observed reflections can be indexed within the crystallographic phase. After the Rietveld refinement, the agreement factors were $\chi^2 = 2.43$, $R_p = 3.52$, $R_{wp} = 4.46$ and $R_I = 5.56$ (in %). No significant decrease was found after including a magnetic phase. Then, the small magnetization observed in the SQUID measurements of this sample arises from magnetically ordered clusters which are not big enough to support a long-range FM ordering suitable to be observed by neutron diffraction. This result is in agreement with the findings in [23, 25, 26] where the percolation threshold for itinerant electrons is proposed to occur in the interval $0.75 < x < 0.85$. That is, at a certain W substitution, the metallic, ferromagnetic patches arising from the Fe–O–Mo–O–Fe interactions become too small, and they are isolated from each other in the insulating, antiferromagnetic matrix created by Fe–O–W–O–Fe superexchange interactions. Then, compositions in the range $0.8 < x < 0.95$ would show the spin-glass behaviour typical of ferromagnetic clusters coupled through an antiferromagnetic matrix [26].

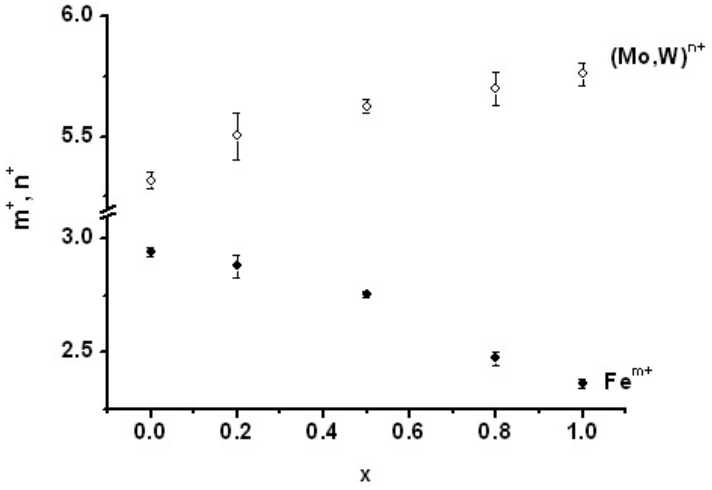

Figure 8. Evolution of the nominal valence states at B′ (Fe) and B″ (Mo,W) sites with the W content x, as calculated from Brown's bond valence model.

Table 2. Main bond distances (Å) and bond angles (deg) for the $Sr_2FeMo_{1-x}W_xO_6$ ($0 \leqslant x \leqslant 1$) series at RT.

Sample	$x = 0$	$x = 0.2$	$x = 0.5$	$x = 0.8$	$x = 1$
$I4/m$			$P2_1/n$		
FeO_6 octahedra					
Fe-O1	2.005(8)	2.02(2)	2.080(4)	2.05(1)	2.077(8)
Fe-O2	1.994(4)	2.00(1)	1.996(5)	2.089(9)	2.086(7)
Fe-O3				1.99(1)	2.074(7)
(Mo, W)O_6 octahedra					
(Mo,W)-O1	1.945(8)	1.94(2)	1.886(4)	1.94(1)	1.930(8)
(Mo,W)-O2	1.955(4)	1.96(1)	1.972(5)	1.93(1)	1.930(7)
(Mo,W)-O3				1.98(1)	1.936(7)
Fe-O1-(Mo,W)	180.0(3)	180.0(9)	180.0(2)	165.2(5)	164.6(3)
Fe-O2-(Mo,W)	171.2(2)	171.0(4)	169.2(2)	163.9(4)	165.1(3)
Fe-O3-(Mo,W)				171.6(4)	166.6(3)

The crystal structure of $Sr_2FeMo_{0.2}W_{0.8}O_6$ at low temperature is monoclinic, and does not show essential changes with respect to the room-temperature one. The lattice parameters are reduced to $a = 5.6236(3)$ Å, $b = 5.5895(3)$ Å and $c = 7.9115(4)$ Å. The monoclinic angle β slightly decreases to $\beta = 90.039(1)°$.

3.3.2. Sr_2FeWO_6. For the determination of the magnetic structure of Sr_2FeWO_6, and the study of its thermal variation, a series of NPD patterns was obtained at the high-flux D20 diffractometer (ILL-Grenoble) with a wavelength of 2.42 Å, in the temperature range from 20 to 70 K in 2 K steps.

In Sr_2FeWO_6, upon decreasing the temperature below the Néel temperature defined by SQUID measurements ($T_N = 38$ K), new reflections appear on positions forbidden for the Bragg crystallographic reflections in the space group $P2_1/n$, as shown in figure 9(a). These new peaks correspond to magnetic reflections accounting for the long range antiferromagnetic ordering of the sample. A fitting of the D20 low-temperature NPD profiles in the pattern

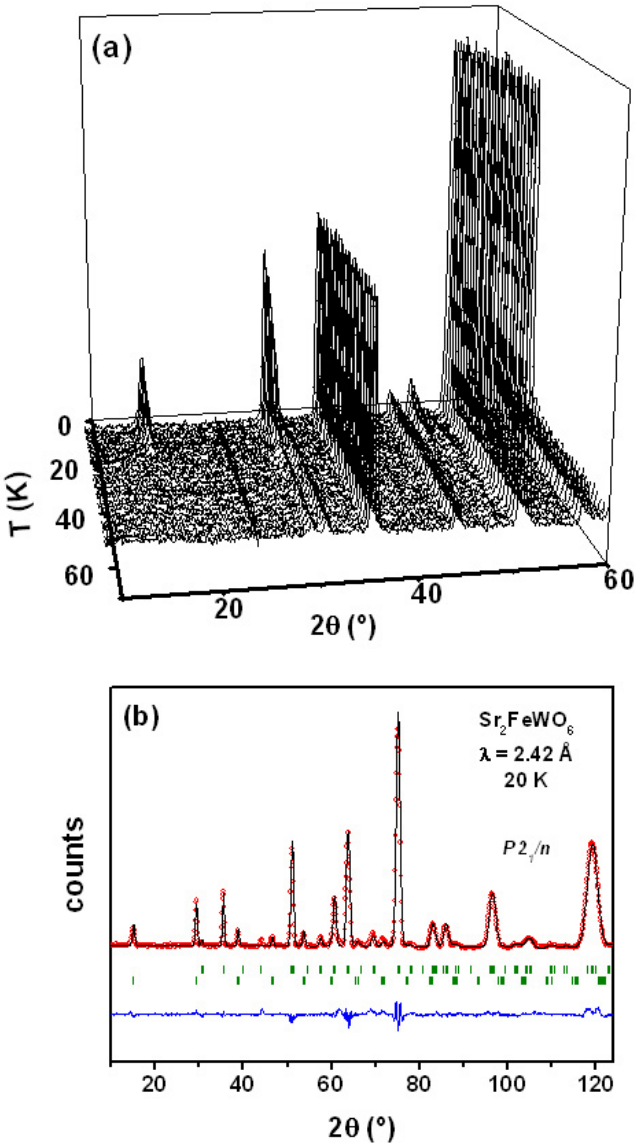

Figure 9. (a) Thermal evolution of the NPD patterns of Sr_2FeWO_6 from 20 to 70 K recorded at 2 K steps at the D20 diffractometer ($\lambda = 2.42$ Å); (b) Rietveld refinement of the Sr_2FeWO_6 crystal and magnetic structure at 20 K.

matching mode of the FullProf program restricts the possible propagation vectors to $\mathbf{k} = (1/2, 0, 1/2)$ and $\mathbf{k} = (0, 1/2, 1/2)$. The antiferromagnetic structure was modelled with magnetic moments at the Fe positions. Sr_2FeWO_6 contains two equivalent Fe atoms at positions 2d ($(1/2, 0, 1/2)$ and $(0, 1/2, 0)$) in the monoclinic unit cell ($P2_1/n$, $Z = 2$). Independently of the propagation vector, the magnetic moments at these positions can be either parallel or antiparallel. After trying different configurations, the best fit was achieved with $\mathbf{k} = (0, 1/2, 1/2)$ and magnetic moments antiferromagnetically aligned in Fe equivalent crystallographic sites. Figure 9(b) shows the goodness of the fit, including the crystal

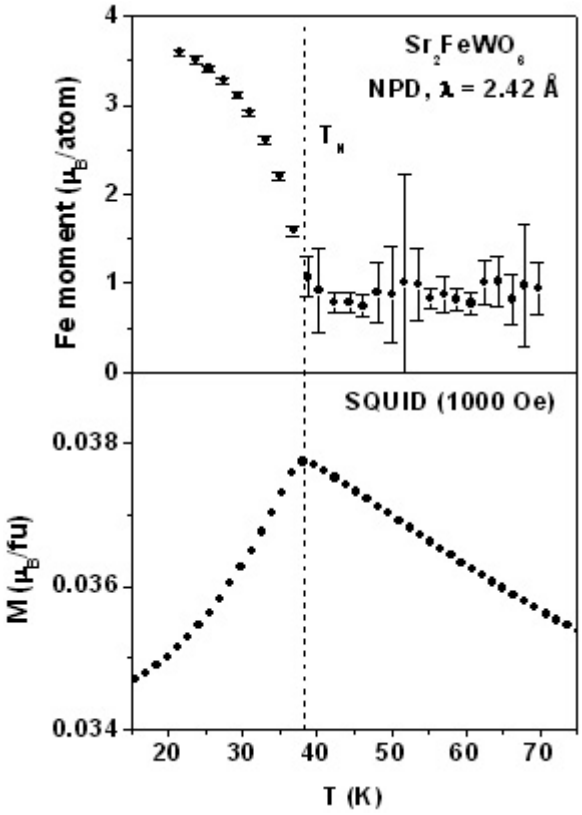

Figure 10. Temperature variation of the ordered magnetic moments on Fe positions in Sr_2FeWO_6 refined from sequential NPD data (upper panel). The T_N defined by NPD is ∼38 K, as also obtained in SQUID measurements (lower panel).

structure (upper series of tick markers) and the magnetic structure (lower series). The components of the Fe magnetic moments at the lower measuring temperature (20 K) were $m_x = -1.93(5)\ \mu_B$/atom, $m_y = -2.4(4)\ \mu_B$/atom and $m_z = 1.8(5)\ \mu_B$/atom. This magnetic structure only differs from the one reported in [31] in the orientation of the magnetic moments, which were found to be roughly aligned with the propagation vector ((011) direction).

The magnetic structure is stable to T_N, as demonstrated in the sequential refinement in the available temperature range. The thermal evolution of the ordered magnetic moment of the Fe positions is shown in the upper panel of figure 10. A sharp increase is observed below 38 K, in coincidence with the maximum in susceptibility (lower panel of figure 10). A value of 3.59(4) μ_B/atom is reached at 20 K. This magnitude represents the ordered magnetic moment on Fe positions, and it is slightly smaller than the spin-only contribution of 4 μ_B/atom for the high-spin Fe^{2+} ($4t_{2g}2e_g$) cation. As is apparent in figure 10, the ordered magnetic moment is still not saturated at the lowest measuring temperature, probably reaching the expected value at a lower T.

4. Conclusions

The structural evolution of the $Sr_2FeMo_{1-x}W_xO_6$ ($0 \leqslant x \leqslant 1$) double perovskites has been investigated by neutron diffraction in complement with magnetic measurements. Only the

samples with x up to 0.5 exhibit a clear FM behaviour, with decreasing T_C values as the W content increases. A reduction in the saturation magnetization is also observed, as a consequence of the appearance of Fe–O–W–O–Fe pairs. At a high substitution level, $x \sim 0.6$, the BO_6 octahedra tilt to relax the bond stress, and the compound undergoes a change of symmetry, from tetragonal ($I4/m$) for lower x values to monoclinic ($P2_1/n$) for high W contents. The driving force of the structural phase transition is the promotion of the voluminous Fe^{2+} cations upon W substitution: the increasing structural stress in the former part of the series is suddenly relieved upon the phase transition, giving rise to a dramatic reduction of the distortion of the BO_6 octahedra. This translates into a distortion of the Sr environment, accommodating the changes in the metal–oxygen octahedra within the 12 Sr–O bonds. The progressive localization of the carriers induces an smooth evolution of the volume and the lattice parameters with the W content.

Acknowledgments

We thank CICyT for the financial support of project MAT 2004-479, and CAM for supporting the project GR/MAT/0427/2004, and we are grateful to ILL for making all facilities available.

References

[1] Sarma D D, Mahadevan P, Saha-Dasgupta T, Ray S and Kumar A 2000 *Phys. Rev. Lett.* **85** 2549
[2] Niebieskikwiat D, Sánchez R D, Caneiro A, Morales L, Vásquez-Mansilla M, Rivadulla F and Hueso L E 2000 *Phys. Rev.* B **62** 03340
[3] Tovar M, Causa M T, Butera A, Navarro J, Martínez B, Fontcuberta J and Passeggi M C G 2002 *Phys. Rev.* B **66** 024409
[4] Fang Z, Terakura K and Kanamori J 2001 *Phys. Rev.* B **63** 180407R
[5] Kang J-S, Han H, Lee B W, Olson C G, Han S W, Kim K H, Jeong J I, Park J H and Min B I 2001 *Phys. Rev.* B **64** 024429
[6] Saitoh T, Nakatake M and Kakizaki A 2002 *Phys. Rev.* B **66** 035112
[7] Ray S, Kumar A, Sarma D D, Cimino R, Turchini S, Zennaro S and Zema N 2001 *Phys. Rev. Lett.* **87** 097204
[8] Aligia A A, Petrone P, Sofo J O and Alascio B 2001 *Phys. Rev.* B **64** 092414
[9] Chattopadhyay A and Millis A J 2001 *Phys. Rev.* B **64** 024424
[10] Ritter C, Ibarra M R, Morellón L, Blasco J, García J and De Teresa J M 2000 *J. Phys.: Condens. Matter* **12** 8295
[11] Frontera C, Rubí D, Navarro J, García-Muñoz J L and Fontcuberta J 2003 *Phys. Rev.* B **68** 012412
[12] Alonso J L, Fernández L A, Guinea F, Lesmes F and Martín-Mayor V 2003 *Phys. Rev.* B **67** 214423
[13] Solovyev I V 2002 *Phys. Rev.* B **65** 144446
[14] Sarma D D 2001 *Curr. Opin. Solid State Mater. Sci.* **5** 261
[15] Navarro J, Frontera C, Balcells Ll, Martínez B and Fontcuberta J 2001 *Phys. Rev.* B **64** 092411
[16] Navarro J, Nogués J, Muñoz J S and Fontcuberta J 2003 *Phys. Rev.* B **67** 174416
[17] Serrate D, De Teresa J M, Blasco J, Ibarra M R, Morellón L and Ritter C 2002 *Appl. Phys. Lett.* **80** 4573
[18] Navarro J, Fontcuberta J, Izquierdo M, Avila J and Asensio M C 2004 *Phys. Rev.* B **69** 115101
[19] Sánchez D, Alonso J A, García-Hernández M, Martínez-Lope M J, Casais M T and Martínez J L 2003 *J. Mater. Chem.* **13** 1771
[20] Moritomo Y, Xu S, Akimoto T, Machida A, Hamada N, Ohoyama K, Takata E N M and Sakata M 2000 *Phys. Rev.* B **62** 14224
[21] Nakawaga T, Yoshikawa K and Nomura S 1969 *J. Phys. Soc. Japan* **27** 880
[22] Kawanaka H, Hase I, Toyama S and Nishihara Y 2000 *Physica* B **281/282** 518
[23] Kobayashi K-I, Okuda T, Tomioka Y, Kimura T and Tokura Y 2000 *J. Magn. Magn. Mater.* **218** 17
[24] Lindén J, Yamamoto T, Nakamura J, Yamauchi H and Karppinen M 2002 *Phys. Rev.* B **66** 184408
[25] Ray S, Kumar A, Majumdar S, Sampathkumaran E V and Sarma D D 2001 *J. Phys.: Condens. Matter* **13** 607
[26] Dass R I and Goodenough J B 2001 *Phys. Rev.* B **63** 064417
[27] Douvalis A P, Venkatesan M, Coey J M D, Grafoute M, Greneche J-M and Suryanarayanan R 2002 *J. Phys.: Condens. Matter* **14** 12611

[28] Retuerto M, Alonso J A, Martínez-Lope M J, Martínez J L and García-Hernández M 2004 *Appl. Phys. Lett.* **85** 266
[29] Rodríguez-Carvajal J 1993 *Physica* B **192** 55
[30] Chmaissem O, Kruk R, Dabrowski B, Brown D E, Xiong X, Kolesnik S, Jorgensen J D and Kimball C W 2000 *Phys. Rev.* B **62** 014197
[31] Azad A K, Eriksson S-G, Mellergard A, Ivanov S A, Eriksen J and Rundlöf H 2002 *Mater. Res. Bull.* **37** 1797
[32] Blasse G 1965 *J. Inorg. Nucl. Chem.* **27** 993
[33] Glazer A M 1972 *Acta Crystallogr.* B **28** 3384
[34] Woodward P M 1997 *Acta Crystallogr.* B **53** 32
[35] Alonso J A, Casais M T, Martínez-Lope M J, Martínez J L, Velasco P, Muñoz A and Fernández-Díaz M T 2000 *Chem. Mater.* **12** 161
[36] Martínez-Lope M J, Alonso J A, Casais M T and Fernández-Díaz M T 2003 *Z. Naturf.* b **58** 127
[37] Shannon R D 1976 *Acta Crystallogr.* A **32** 751
[38] Brown I D 1981 *Structure and Bonding in Crystals* vol 2 (New York: Academic)
[39] Brese N E and O'Keeffe M 1991 *Acta Crystallogr.* B **47** 192